Materialia 22 (2022) 101434

Contents lists available at ScienceDirect

Materialia

journal homepage: www.elsevier.com/locate/mtla

Thermal stability of a cathodic arc evaporated $Cr_{0.74}Ta_{0.26}N$ coating

Christina Kainz[a,*], Michael Tkadletz[b], Andreas Stark[c], Norbert Schell[c], Christoph Czettl[d], Markus Pohler[d], Nina Schalk[a]

[a] Christian Doppler Laboratory for Advanced Coated Cutting Tools at the Department of Materials Science, Montanuniversität Leoben, Franz-Josef-Straße 18, Leoben 8700, Austria
[b] Department of Materials Science, Montanuniversität Leoben, Franz-Josef-Straße 18, Leoben 8700, Austria
[c] Institute of Materials Physics, Helmholtz-Zentrum Hereon, Max-Planck-Straße 1, Geesthacht 21502, Germany
[d] Ceratizit Austria GmbH, Metallwerk-Plansee-Straße 71, Reutte 6600, Austria

ARTICLE INFO

Keywords:
CrTaN
Cathodic arc evaporation
Thermal stability
Synchrotron radiation
Atom probe tomography

ABSTRACT

CrTaN coatings have recently received increasing industrial interest due to their combination of high hardness, promising fracture toughness and excellent oxidation resistance. However, up to now no thorough investigation on the thermal stability of this coating system is available. Thus, within this work, the evolution of the microstructure and phase composition of an arc evaporated CrTaN coating were illuminated in inert atmosphere up to 1400°C. The coating crystallizes in an fcc-$Cr_{0.74}Ta_{0.26}N$ solid solution with a preferred <311> orientation. Alternating Cr-enriched and Ta-enriched layers are identified in the cross-section of the as-deposited coating, which arise from the three-fold rotation during deposition. *In-situ* high energy X-ray diffraction showed that powdered CrTaN is stable in inert atmosphere up to ~1250°C, where fcc-$Cr_xTa_{1-x}N$ starts to transform into t-$Cr_{1.2}Ta_{0.8}N$. Upon further increasing the temperature to values exceeding 1300°C, h-Cr_2N and h-Ta_5N_4 start to form. Vacuum annealing of a CrTaN coating on a sapphire substrate at 1000°C results in the homogenization of the synthesis-related compositional fluctuations. While still maintaining the fcc-$Cr_xTa_{1-x}N$ solid solution, a texture change to a preferred <100> orientation is observed after annealing at 1270°C. An annealing treatment at 1300°C results in the formation of t-$Cr_{1.2}Ta_{0.8}N$ in addition to the fcc-$Cr_{1-x}Ta_xN$.

1. Introduction

CrN based hard coatings grown by physical vapor deposition (PVD) are established materials for applications in harsh conditions. Here, especially CrAlN has been extensively studied within the last decades, owing to its high hardness and excellent oxidation resistance [1–3]. Contrary, CrTaN coatings have only recently been identified as a promising candidate for severe applications such as metal cutting. Although the hexagonal (h) TaN modifications are thermodynamically favored over the cubic one [4], face-centered cubic (fcc) $Cr_xTa_{1-x}N$ can be synthesized by PVD due to the non-equilibrium conditions of the process [5–9]. Adjusting the Cr/(Cr+Ta) ratio in the coating allows to tailor the properties for the desired application: while the hardness increases with increasing Ta content [5], an improved oxidation resistance is reported in coatings with a high Cr content [7]. In addition to the chemical composition, also the deposition parameters determine the microstructure and mechanical properties of the coatings. The authors observed in a previous study that an increasing bias voltage results not only in higher hardness, but also in a higher fracture toughness of CAE CrTaN coatings [10].

The thermal decomposition of CrN based coatings is well reviewed in literature [11–13]. Ernst et al. reported that the decomposition of the fcc-CrN phase to h-Cr_2N starts at ~940°C, followed by a decomposition to body-centered cubic (bcc) Cr at ~1100°C [11]. The accompanying formation of gaseous N_2 and the volume change result in pores, deteriorating the mechanical properties. Adding Al or Si to CrN significantly improves its thermal stability and has thus been thoroughly investigated in the past [1,2,14]. In contrast, little information can be found on how the presence of Ta influences the decomposition of CrN at elevated temperatures. Contrary to metastable CrAlN and CrSiN [15], fcc-CrN and fcc-TaN are miscible throughout the whole compositional range [16], which suggests a high thermal stability of this coating system. In a previous work, the authors investigated the thermal stability of powdered CrTaN and observed the formation of nitrogen-deficient compounds at temperatures >1200°C [10]. However, the detailed decomposition sequence of fcc-$Cr_xTa_{1-x}N$ remains unclear. Furthermore, literature on the influence of the thermal stability on the mechanical properties of CrTaN is scarce [5,10].

Thus, the aim of this work is to shed light on the evolution of the phase composition and microstructure of an arc evaporated CrTaN

* Corresponding author.
E-mail address: christina.kainz@unileoben.ac.at (C. Kainz).

https://doi.org/10.1016/j.mtla.2022.101434
Received 23 February 2022; Accepted 20 April 2022
Available online 25 April 2022

coating upon annealing in inert atmosphere. *In-situ* synchrotron X-ray diffraction (XRD) was applied to study the thermal stability of powdered CrTaN between 100 and 1400°C. Differential scanning calorimetry (DSC) as well as thermo-gravimetric analysis (TGA) supplemented the XRD investigation. The phase composition and microstructure of CrTaN on sapphire after annealing at selected temperatures were investigated in a combinatorial approach of XRD, scanning electron microscopy (SEM), energy-dispersive X-ray spectroscopy (EDX) and atom probe tomography (APT). Finally, nanoindentation allowed to correlate the microstructure of the vacuum annealed samples with their mechanical properties.

2. Experimental methods

The coatings investigated in this study were grown by means of CAE in an industrial scale Oerlikon Balzers INNOVA arc evaporation system. Three powder metallurgically produced compound targets of 75 at.% Cr and 25 at.% Ta were used as source material. The deposition was conducted in pure N_2 atmosphere (3.3×10^{-2} mbar) at a substrate temperature of 450°C and a bias voltage of -60 V. Mild steel foil and single crystalline sapphire with (001) orientation served as substrates. While the sapphire substrates underwent three-fold rotation within the carousel, the mild steel foil was subjected to two-fold rotation. The latter one was dissolved after deposition using diluted HNO_3 to obtain coating powder. Both, glow discharge optical emission spectroscopy (GDOES) as well as EDX were applied to quantify the chemical composition. While a GD-Profiler 2 by Horiba was used for the GDOES measurement, EDX was realized on an Ultim Max detector by Oxford instruments attached to a scanning electron microscope (SEM) type Clara from Tescan. The microstructure of the powdered coating and the CrTaN on sapphire was investigated by lab-scale XRD on a Bruker AXS D8 Advance diffractometer utilizing CuK_α radiation. The measurements were performed in Bragg-Brentano geometry. Applying the $\sin^2\psi$ method allowed to quantify the residual stress of the CrTaN on sapphire. The analysis was performed in side-inclination on the 311 reflection with $\sin^2\psi$ inclinations varying between 0 and 0.55. The X-ray elastic constants were calculated from the constants of fcc-CrN [17] and fcc-TaN [18] applying the Hill-Grain interaction model. XRD pole figures were recorded from the 111, 200, 220 and 311 reflections within an azimuthal and polar angle range from 0-360° and 0-80°, respectively. The MTEX toolbox allowed to process the data and visualize the re-calculated pole figures as well as the inverse pole figures [19].

The *in-situ* synchrotron experiments were carried out at the high energy materials science beamline P07 at PETRA III, Helmholtz-Zentrum Hereon [20]. A beam wavelength of 0.11965 Å, corresponding to an energy of 103.6 keV, was selected. A Pt crucible containing the powdered coating material was inductively heated from 100 to 1400°C at a heating rate of 20°C/min. 2D X-ray diffractograms in Debye-Scherrer geometry were recorded every ~5°C with a digital X-ray detector Perkin Elmer XRD 1621. The Debye-Scherrer rings were then azimuthally integrated using the software Dawn 2 to obtain one-dimensional diffractograms [21]. The subsequent sequential Rietveld refinement for each diffraction pattern was realized using the software TOPAS 6 by Bruker [22]. For further details on the procedure of the refinement, the reader is referred to ref. [23]. The used crystallographic information files of fcc-CrN (1008956), fcc-TaN (2310957), tetragonal (t) $Cr_{1.2}Ta_{0.8}N$ (2106680), h-Cr_2N (4311894) and h-Ta_5N_4 (1538016) can be found in the Crystallography Open Database. DSC/TGA experiments on CrTaN powders were conducted on a Setaram Setsys EVO 2400 calorimeter. The measurement was performed in Ar and a maximum temperature of 1400°C and a heating rate of 20°C/min were applied.

Annealing experiments in vacuum were realized using a HTM Reetz vacuum furnace operating at a base pressure $<5 \times 10^{-6}$ mbar with the same heating rate as applied in the synchrotron experiment (20°C/min). The annealing temperatures were set to 1000, 1270 and 1300°C, respectively and were held for 5 minutes. A virgin sample was used for every heat treatment. As for the as-deposited coatings, the microstructure of the annealed samples was investigated by XRD using the aforementioned diffractometer by Bruker. Cross-sectional secondary electron micrographs of the as-deposited and annealed coatings were obtained using a field emission gun scanning electron microscope. APT specimen were fabricated from the as-deposited coating as well as from the coating annealed at 1000°C applying the lift-out technique [24]. For the measurements of the specimen, a local electrode atom probe LEAP 3000X HR from CAMECA was used. The experiments were performed in laser-assisted mode at a temperature, laser energy and pulse rate of 60 K, 0.6 nJ per pulse and 250 kHz, respectively. In case of the coating annealed at 1300°C, a cross-sectional EDX mapping was carried out with a scanning electron microscope type Gemini 450 from Zeiss. The microscope is equipped with an Ultim Extreme EDX detector by Oxford Instruments. The coating hardness and Young's modulus were determined in continuous stiffness mode on a G200 nanoindenter from KLA, equipped with a Berkovich tip. Taking into account a Poisson's ratio of 0.27, the hardness and Young's modulus of the coatings were calculated from an indentation depth of 100-150 nm applying the Oliver and Pharr method [25].

3. Results and discussion

3.1. Coating in as-deposited state

The elemental composition of the investigated coating was determined to 37 at.% Cr, 13 at.% Ta and 50 at. % N by means of GDOES. Therefore, the Cr/(Cr+Ta) ratio of 0.74 in the coating is comparable to the one in the target (0.75). Within the accuracy of the measurement, a comparable Cr/(Cr+Ta) ratio (0.76) was determined by EDX. In Fig. 1a, the X-ray diffractograms of the powdered coating and CrTaN on sapphire are presented. The authors decided to use the d-spacing rather than the 2θ angle, as the diffractograms recorded in the laboratory and at the synchrotron radiation facility were obtained at different wavelengths. Since the reflections of the investigated CrTaN powder and coating lie between those reported for fcc-CrN [26] and fcc-TaN [27], it can be concluded that an fcc-$Cr_{0.74}Ta_{0.26}N$ solid solution has formed. The reflections of CrTaN on sapphire are slightly shifted to larger d-spacings as compared to those of the powder. This deviation is ascribed to the compressive residual stress of the coating on sapphire, which was determined to -3.0±0.3 GPa. The 311 reflection is most pronounced in case of CrTaN on sapphire, which is in contrast to the powder, where the 200 reflection exhibits the highest intensity. Since this fact indicates a preferred orientation in the CrTaN coating on sapphire, XRD pole figures were recorded. The calculated inverse pole figure in growth direction (Fig. 1b) confirms the pronounced <311> preferred orientation, whereas also contributions from the <100> and <111> orientations are apparent.

A cross-sectional micrograph of the CrTaN coating on sapphire is shown in Fig. 1c. The coating consists of elongated grains, which do not extend over the whole coating thickness. An increasing grain size with increasing coating thickness can be observed, which is a typical characteristic of competitive growth [28]. It is furthermore evident that the chemical composition in the coating is not homogenous, since the phase contrast changes periodically throughout the coating thickness. This observation is attributed to compositional heterogeneous layers, which are reported to form as a result of the three-fold rotation during deposition [29].

To obtain a more detailed understanding of the compositional heterogeneous layers within the coating on sapphire, APT was applied. The specimen reconstruction with the atom maps of Cr, Ta and N in Fig. 2a confirms the presence of a layered structure. Additionally, isoconcentration surfaces of 39 at.% Cr and 12 at.% Ta are shown to provide a better visualization of the layered structure. While N is homogeneously distributed throughout the specimen, an inhomogeneity in the Cr and Ta

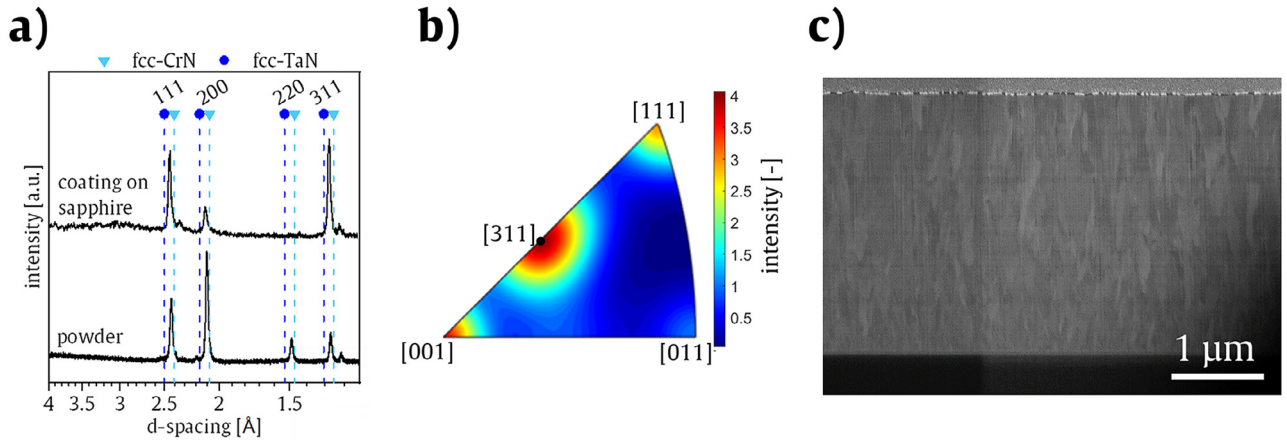

Fig. 1. (a) X-ray diffractogram of CrTaN on sapphire in the as-deposited state. The X-ray diffractogram of powdered CrTaN is shown as well. (b) Inverse XRD pole figure, calculated in growth direction, of the coating on sapphire. (c) Cross-sectional scanning electron micrograph of CrTaN on sapphire.

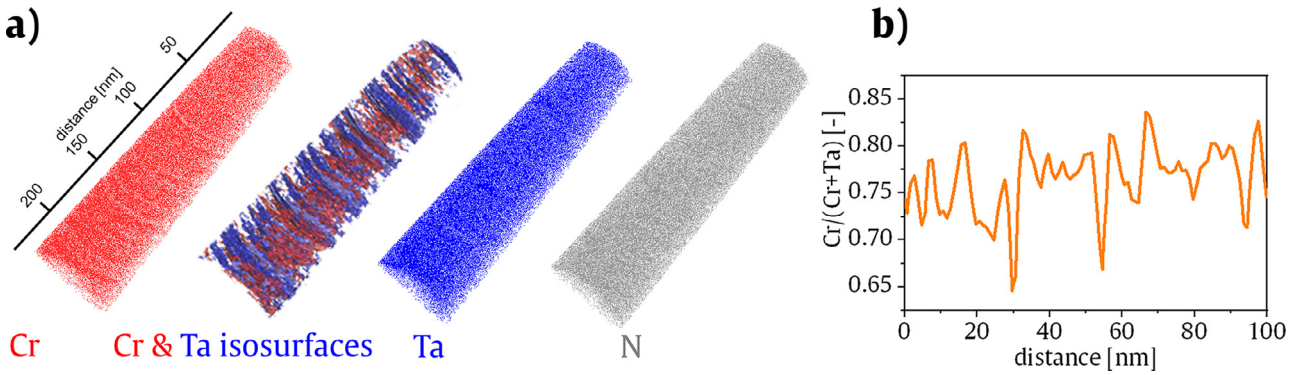

Fig. 2. (a) Cr (red), Ta (blue) and N (grey) atom map of an APT measurement on the as-deposited coating. The atom maps show 2.5, 19 and 3 % of the detected Cr, Ta and N ions, respectively. An isoconcentration surface representation of 39 at.% Cr and 12 at.% Ta is shown as well. (b) The Cr/(Cr+Ta) ratio along the growth direction of the coating. (For interpretation of the references to color in this figure legend, the reader is referred to the web version of this article.).

distribution is evident. From a compositional profile along the growth direction of the coating (Fig. 2b), the Cr/(Cr+Ta) ratio was found to vary between a maximum of 0.83 and a minimum of 0.65. The modulation period of the layers was determined to 5.3±1.7 nm from the APT experiment. It is evident from Fig. 2b that both, the Cr/(Cr+Ta) ratio in the respective layer as well as the modulation period differs from one Cr-richer layer to the subsequent one. This fact can be attributed to the three-fold rotation, which results in a lower homogeneity of the layer composition and thickness as compared to the one- or two-fold rotation [30].

3.2. Thermal stability of coating powder

To illuminate the temperature-dependent phase composition of powdered CrTaN upon annealing, high-energy XRD experiments at a synchrotron radiation facility were conducted. The phase evolution with respect to the temperature as derived from the synchrotron experiment is shown in Fig. 3a. In order to allow for a more detailed view of the ongoing reactions at elevated temperature, the phase plot is shown in a temperature regime from 800 to 1400°C. Reflections stemming from the Pt crucible have been removed in a first refinement step and are thus not included. The phase plot can be divided into three temperature zones, separated by horizontal dashed lines within the figure. At the border of each zone, new phases form or existing phases vanish. Up to ~1250°C (zone 1), no additional phases to the fcc-$Cr_xTa_{1-x}N$ solid solution contribute to the phase composition. The diffraction peaks of the fcc-$Cr_xTa_{1-x}N$ solid solution shift to larger d-spacings as the temperature increases up to ~1170°C. This observation can be attributed to the thermal expansion of the lattice and the resulting increment of the lattice parameter. As the temperature is further increased, however, the reflections of the fcc-$Cr_xTa_{1-x}N$ solid solution shift to lower d-spacings towards the standard peak positions of fcc-CrN within zone 2. Furthermore, the formation of an additional phase starts slightly delayed at ~1250°C, which is attributed to t-$Cr_{1.2}Ta_{0.8}N$ [31]. With this transformation onset temperature, CrTaN outperforms the thermal stability of CrN and CrAlN by 250 and 100°C, respectively [11,32]. The formation of t-$Cr_{1.2}Ta_{0.8}N$ is in agreement with Hu et al., who observed this compound as a thermal decomposition product of CrAlTaN coatings [33]. The Cr/(Cr+Ta) ratio in t-$Cr_{1.2}Ta_{0.8}N$ amounts to 0.6 and is thus lower compared to the one in the initial fcc-$Cr_xTa_{1-x}N$ solid solution (0.74). Hence, the remaining fcc-$Cr_xTa_{1-x}N$ solid solution is rich in Cr, which explains the shift of the XRD reflections towards the peak position of fcc-CrN. To further support the suggestion that t-$Cr_{1.2}Ta_{0.8}N$ is predominant at 1300°C, pristine CrTaN powder was annealed within a vacuum furnace to this temperature. The annealed powder consists of 43 at.% Cr, 26 at.% Ta and 31 at.% N according to EDX, which is in fair agreement with the reported composition of t-$Cr_{1.2}Ta_{0.8}N$ [31]. Reflections stemming from t-$Cr_{1.2}Ta_{0.8}N$ vanish as the temperature exceeds 1300°C and instead, h-Cr_2N [34] and h-Ta_5N_4 [35] form within zone 3. The formation of h-Cr_2N and h-Ta_5N_4 upon heating fcc-$Cr_xTa_{1-x}N$ to temperatures exceeding 1200°C is in agreement to literature [10,36]. To study the thermal decomposition in more detail and to quantify the phase

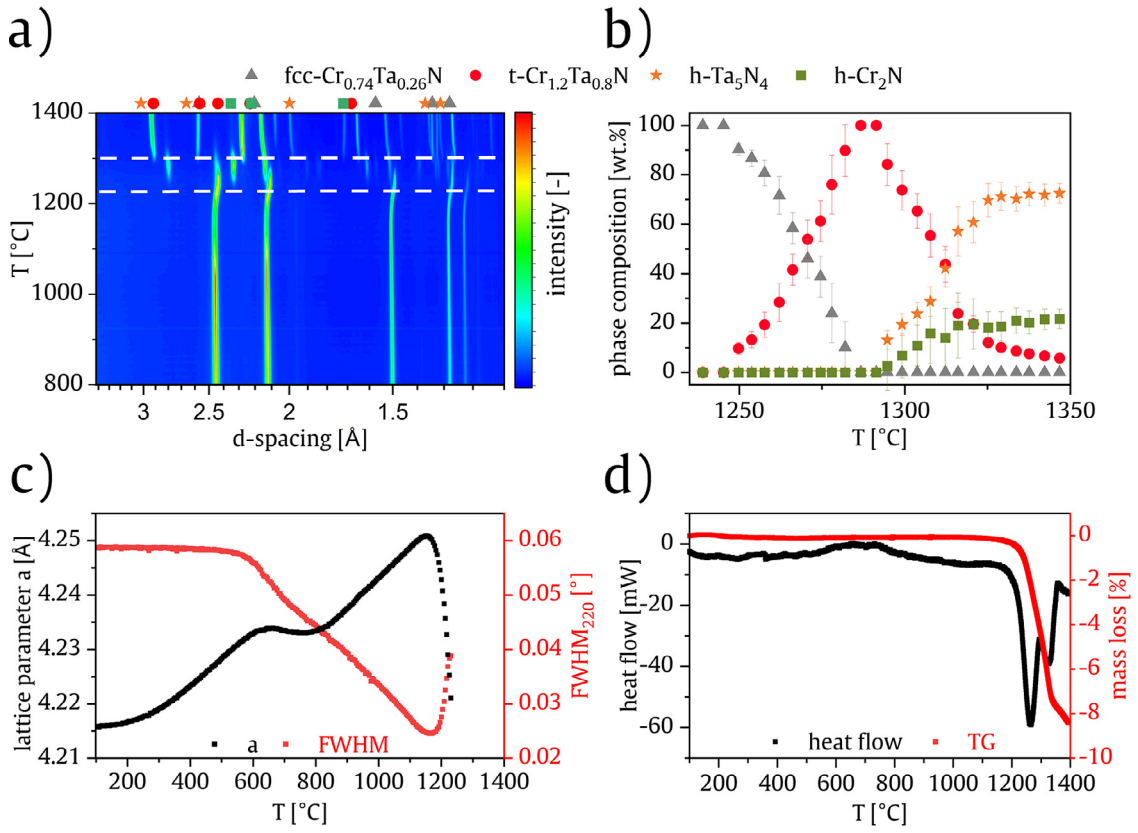

Fig. 3. (a) Phase evolution of powdered CrTaN in vacuum between 800 and 1400°C. The standard peak positions of fcc-$Cr_{0.74}Ta_{0.26}N$, t-$Cr_{1.2}Ta_{0.8}N$, h-Ta_5N_4 and h-Cr_2N at RT are given as well. (b) Quantitative phase composition of the CrTaN powder as a function of the temperature as determined by quantitative Rietveld refinement. (c) Evolution of the lattice parameter and the FWHM from 100 to 1250°C. (d) Heat flow and mass change determined from a DSC/TGA experiment supplementing the crystallographic investigation.

fraction of the respective phases, sequential Rietveld refinement was applied. The results of this investigation are shown in Fig. 3b. Prior to 1250°C, only the fcc-$Cr_xTa_{1-x}N$ phase can be determined. As the temperature further increases, the phase fraction of t-$Cr_{1.2}Ta_{0.8}N$ rises up to 1300°C, where only this compound is detected. Between 1300 and 1400°C, the fraction of t-$Cr_{1.2}Ta_{0.8}N$ decreases in favor of h-Cr_2N and h-Ta_5N_4.

From the peak positions determined by the sequential Rietveld refinement, the evolution of the lattice parameter with increasing temperature can be obtained (Fig. 3c). Up to ~600°C, the lattice parameter of CrTaN increases due to the thermal expansion of the material. Between 600 and 800°C, however, the lattice parameter stays constant, before it increases again between 800 and 1170°C. It is suggested that this phenomenon relies on the fact that CrTaN exhibits a negative mixing enthalpy regardless of the Cr/(Cr+Ta) ratio [16]. There is thus a high driving force for the compositional heterogeneous nano-layers (cf. Figs. 1c and 2) to dissolve in favor of a homogenous composition. Prior to the intermixing, the evolution of the lattice parameter can be understood as a superimposition of the thermal expansion resulting from layers with varying composition. Upon loss of the layers, the Cr/(Cr+Ta) ratio becomes homogenous within the investigated powder, resulting in a change of the thermal expansion. In agreement, the authors observed the loss of the nano-layered structure after annealing CrTaN on cemented carbide for 2 hours at 900°C in a previous work [10]. As the temperature exceeds 1170°C, the lattice parameter decreases significantly with increasing temperature owing to the enrichment of Cr in the fcc-$Cr_xTa_{1-x}N$ solid solution. In addition to the evolution of the lattice parameter, the influence of the temperature on the XRD peak broadening is shown in Fig. 3c. The full width at half maximum (FWHM) was evaluated by fitting the fcc-$Cr_xTa_{1-x}N$ 220 diffraction peak applying the Pseudo-Voigt function. A larger FWHM indicates a smaller size of the coherently diffracting domains and more pronounced micro-strain [37]. Up to a temperature of ~600°C, the FWHM stays constant. As the temperature increases further, the FWHM decreases, which indicates domain growth and annihilation of micro-strain. The suggested homogenization of the nano-layers thus seems to induce a reduction of the microstructural defects. At 1180°C, the FWHM reaches its minimum, before it slightly increases again as the temperature further increases. It is suggested that the fcc→t-CrTaN phase transformation is accompanied by microstructural rearrangements and formation of defects, which increase the FWHM.

A DSC/TGA experiment in Ar complemented the XRD investigation at the synchrotron radiation facility. Fig. 3d shows the heat flow and mass change signal of powdered CrTaN as a function of the temperature. The minor exothermic contribution in the heat flow curve (~600-800°C) is ascribed to the suggested homogenization of the chemical composition. Two pronounced endothermic peaks are visible in the heat flow curve with their maxima at ~1250°C and 1380°C, respectively. The presence of two maxima indicates a two-step reaction, which is in agreement with the decomposition sequence observed in the synchrotron experiments. At the respective on-set temperature of the peaks, the slope of the TGA signal changes as well. The first endothermic peak is attributed to the transformation of the fcc-$Cr_xTa_{1-x}N$ solid solution into t-$Cr_{1.2}Ta_{0.8}N$. Upon further increasing the temperature to ~1300°C, a second, less pronounced peak emerges. This reaction is ascribed to the formation of h-Cr_2N and h-Ta_5N_4. Owing to the formation of nitrogen deficient compounds, N_2 evaporates, which results in an overall mass loss of ~8.5 %.

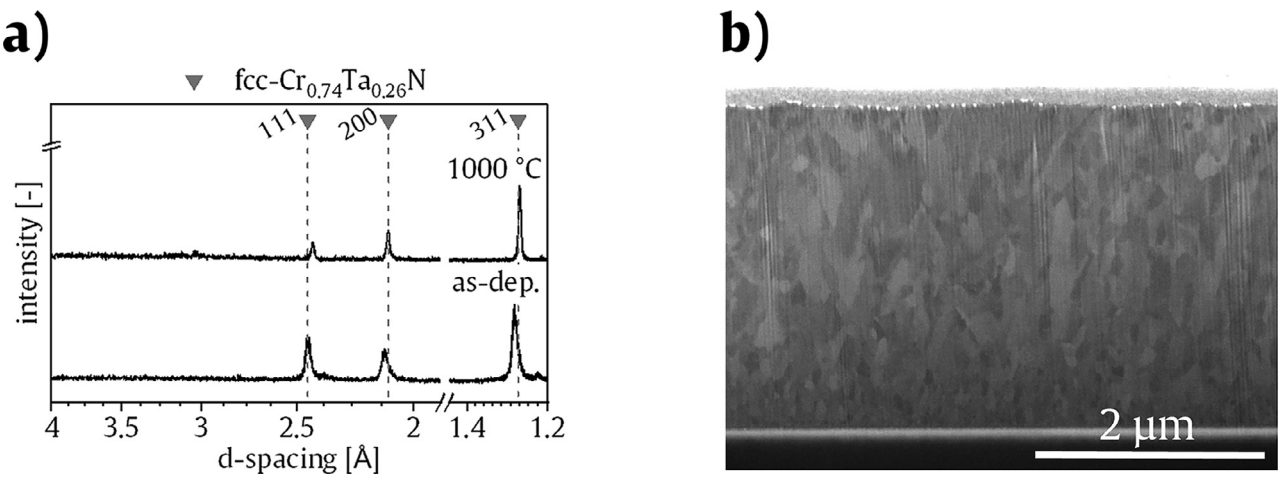

Fig. 4. (a) X-ray diffractogram of CrTaN on sapphire after annealing at 1000°C. The diffractogram of the coating in as-deposited state is shown again to facilitate the comparison. (b) Cross-sectional scanning electron micrograph of the coating after annealing at 1000°C.

3.3. Thermal stability of coating on sapphire

To study the thermal stability of the compact CrTaN coating on sapphire, one sample each was annealed at 1000, 1270 and 1300°C, respectively. For brevity, the samples are denoted by the respective annealing temperature, thus, e.g. CrTaN-1000 was annealed at 1000°C. According to EDX, the elemental composition of CrTaN-1000 amounts to 39 at.% Cr, 13 at.% Ta and 48 at.% N, which is in good agreement with the composition determined for the as-deposited coating. As can be seen from the diffractograms in Fig. 4a, the phase composition of CrTaN is not affected by an annealing treatment at 1000°C. The diffraction peaks of the fcc-$Cr_xTa_{1-x}N$ solid solution in CrTaN-1000 are, however, narrower compared to the as-deposited sample, indicating grain growth and annihilation of defects. Furthermore, the XRD reflections have shifted to lower d-spacings in the annealed coating in comparison to the as-deposited one, which suggests relaxation of the compressive residual stress. Indeed, a $\sin^2\psi$ investigation confirmed a change of the compressive residual stress from -3.0±0.3 GPa in the as-deposited coating to 0.5±0.3 GPa in CrTaN-1000. Fig. 4b shows a cross-sectional micrograph of CrTaN-1000. The grains appear slightly coarser as compared to the as-deposited state (cf. Fig. 1c). This observation is in agreement with the decreasing peak width of the XRD reflections observed for the coating annealed at 1000°C. In contrast to the as-deposited state, CrTaN-1000 does not display the presence of layers in the cross-section anymore. The loss of the layered structure supports the aforementioned assumption that the kink in the lattice parameter (Fig. 2b) can be attributed to inter-diffusion between the layers of varying composition. It should be stressed here that the powder and the coating on sapphire were subjected to two- and three-fold rotation on the carousal, respectively. Thus, dissimilarities in the intermixing behavior regarding e.g. the intermixing onset temperature, cannot be excluded due to differences in the layer periodicity. Nevertheless, regardless of the varying bilayer period, intermixing of the layers at elevated temperature is due to the high thermodynamic driving force expected for both, the CrTaN powder and the intact coating [16].

To study the loss of the layers upon annealing in more detail, an APT investigation of CrTaN on sapphire annealed at 1000°C was carried out. Fig. 5a shows the reconstruction of the specimen with the atom maps of Cr, Ta and N. In contrast to the as-deposited coating (Fig. 2a), a homogeneous distribution of all included elements throughout the specimen is evident in CrTaN-1000. This observation is substantiated by the compositional profile throughout a cylindrical region of interest along the growth direction of the coating. As can be seen in Fig. 5b, annealing at 1000°C resulted in a homogenization of the Cr/(Cr+Ta) ratio throughout the material as compared to the as-deposited state. EDX measurements indicated no influence of an annealing treatment at 1000°C on the elemental composition of the coating. This fact is corroborated by APT, where for both, the as-deposited coating and CrTaN-1000, an overall Cr/(Cr+Ta) ratio of ~0.76 was determined. Summarizing, the loss of the layers upon heating CrTaN to 1000°C as evidenced by SEM and APT strongly supports the aforementioned assumption that the kink in the lattice parameter can be attributed to the homogenization of the Cr/(Cr+Ta) ratio throughout the coating.

The X-ray diffractogram of CrTaN-1270, along with the one of the as-deposited coating is shown in Fig. 6a. Again, no difference in the phase composition is evident. This observation is in contrast to the behavior of the powder (Fig. 3), where at 1270°C already a significant amount of the t-$Cr_{1.2}Ta_{0.8}N$ phase was observed. It is suggested that the lower free surface area in case of the compact coating compared to the powder explains this deviation. Since the fcc→t-CrTaN phase transformation is accompanied by N_2 evaporation, the process is facilitated in the powdered coating. Koller et al. report on a similar behavior in TaAlN coatings, where the formation of N-deficient compounds was observed at a lower temperature in case of the powder as compared to the compact coating [38]. CrTaN-1270 exhibits narrower XRD reflections in comparison to the as-deposited coating, which indicates grain growth. The 200 reflection is most pronounced in CrTaN-1270, whereas in the as-deposited coating and CrTaN-1000 the 311 reflection is dominant. To investigate the effect of annealing at 1270°C on the texture of the coating, XRD pole figure measurements were conducted. The calculated inverse pole figure of CrTaN-1270 in growth direction is shown in Fig. 6b. While the coating in the as-deposited state exhibited a preferred <311> orientation (Fig. 1b), a texture change towards a preferred <200> orientation is evident after annealing at 1270°C. In case of fcc-CrN based materials, the <200> orientation exhibits the lowest surface energy [39]. It is thus suggested that at the given temperature the microstructure is governed by the surface energy. Fig. 6c shows a cross-sectional micrograph of CrTaN-1270. In comparison to the as-deposited state (Fig. 1c) and CrTaN-1000 (Fig. 5b), the grains are significantly coarser after annealing CrTaN at 1270°C. Again, EDX does not indicate a change in the elemental composition of CrTaN-1270 compared to as-deposited CrTaN.

After annealing CrTaN on sapphire at 1300°C, a change of the phase composition becomes evident, as can be seen in Fig. 7a. In agreement with the evolution of the phase composition of powdered CrTaN, t-$Cr_{1.2}Ta_{0.8}N$ forms as decomposition product of the fcc-$Cr_xTa_{1-x}N$ solid solution. Reflections stemming from the fcc-$Cr_xTa_{1-x}N$ solid so-

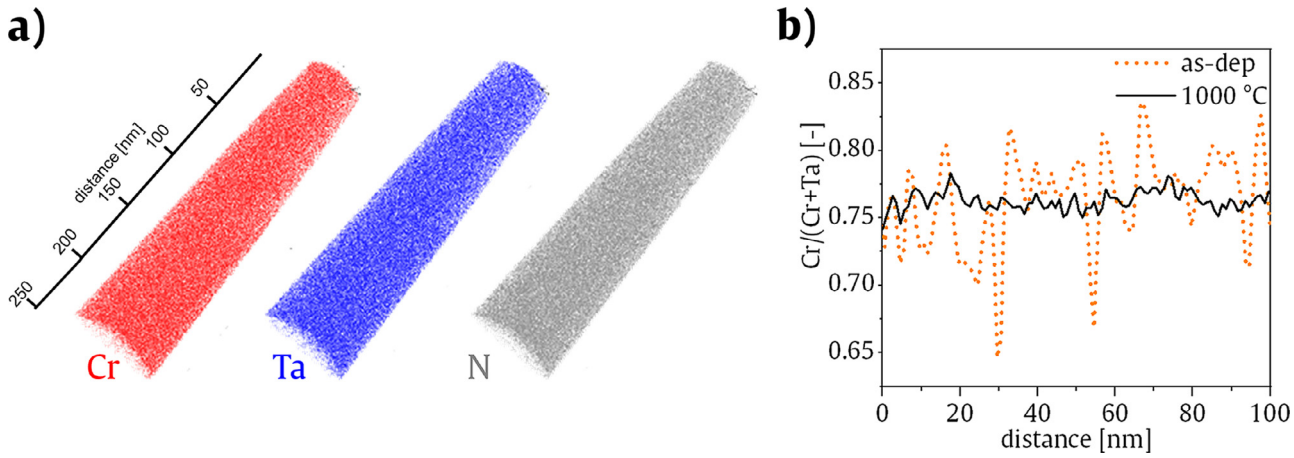

Fig. 5. (a) Cr (red), Ta (blue) and N (grey) atom map of an APT measurement on CrTaN-1000. The atom maps show 1.5, 11 and 3 % of the detected Cr, Ta and N ions, respectively. (b) Cr/(Cr+Ta) ratio along the growth direction of CrTaN-1000. The Cr/(Cr+Ta) ratio determined from a specimen of the as-deposited coating (orange) is shown again to facilitate the comparison. (For interpretation of the references to color in this figure legend, the reader is referred to the web version of this article.)

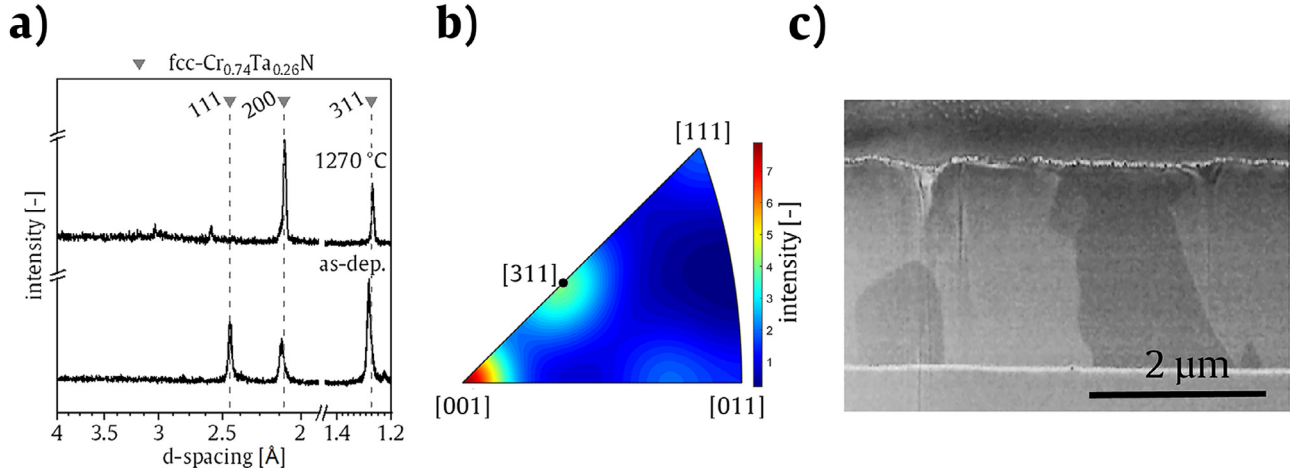

Fig. 6. (a) X-ray diffractogram of CrTaN on sapphire after annealing at 1270°C. The diffractogram of the coating in as-deposited state is shown again to facilitate the comparison. (b) Inverse XRD pole figure, calculated in growth direction, and (c) cross-sectional scanning electron micrograph of the coating annealed at 1270°C.

lution and the t-$Cr_{1.2}Ta_{0.8}N$ contribute to the diffractogram of CrTaN-1300. The presence of a dual-phase structure is also evidenced by the cross-sectional micrograph of CrTaN-1300 in Fig. 7b. Herein, domains corresponding to the intact fcc-$Cr_xTa_{1-x}N$ solid solution coexist with t-$Cr_{1.2}Ta_{0.8}N$ domains. As mentioned above, the Cr/(Cr+Ta) ratio decreases from 0.74 in the fcc-$Cr_xTa_{1-x}N$ solid solution to 0.6 in t-$Cr_{1.2}Ta_{0.8}N$. Thus, darker domains within the secondary electron micrograph correspond to Cr-richer fcc-$Cr_xTa_{1-x}N$, bright ones to Ta-richer t-$Cr_{1.2}Ta_{0.8}N$. This fact is furthermore substantiated by the EDX elemental maps of Cr, Ta and N in Fig. 7c. Within the t-$Cr_{1.2}Ta_{0.8}N$ domain, Ta is enriched and N is reduced as compared to the intact fcc-$Cr_xTa_{1-x}N$ domain. Cr appears homogeneously distributed throughout both domains. This fact is in agreement to theoretical considerations, since the overall Cr content in t-$Cr_{1.2}Ta_{0.8}N$ (40 at.%) is comparable to the one in the fcc-$Cr_xTa_{1-x}N$ solid solution (37 at.%).

The structural evolution of the coating during annealing significantly influences the mechanical properties of the material as shown in Fig. 8. CrTaN exhibits a hardness of 29.4±1.7 GPa in the as-deposited state, which is in fair agreement with values reported in literature [8,10]. Annealing at 1000 and 1270°C results in a reduction of the hardness to 26.2±0.5 GPa and 26.8±0.6 GPa, respectively. The hardness loss upon annealing can be attributed both, to a reduction of the compressive residual stress and grain coarsening. Annealing the coating at 1300°C and the accompanied formation of t-$Cr_{1.2}Ta_{0.8}N$ provokes a reduction of the hardness to 23.6±0.7 GPa. This observation is in agreement with Hu et al., who observed that the formation of t-$Cr_{1.2}Ta_{0.8}N$ in annealed CrAlTaN coatings is accompanied by a hardness decrease [33]. In addition to the hardness, also the Young's modulus displays a strong dependence on the annealing temperature. The reduction of the Young's modulus from 445±18 GPa in the as-deposited state to 407±29 GPa in case of CrTaN-1000 can again be ascribed to the relaxation of the compressive residual stress. CrTaN-1270 exhibits a higher Young's modulus of 479±9 GPa as compared to the as-deposited state and CrTaN-1000. This behavior can be attributed to the texture change upon annealing: the as-deposited coating exhibits a preferred <311> orientation, whereas the grains in CrTaN-1270 are largely <100> oriented. In fcc-based materials, the theoretical Young's modulus is highest in the <100> direction [40]. As a result of the fcc→t-CrTaN phase transformation after annealing at 1300°C, a reduction of the Young's modulus to 362±26 GPa is evident [33].

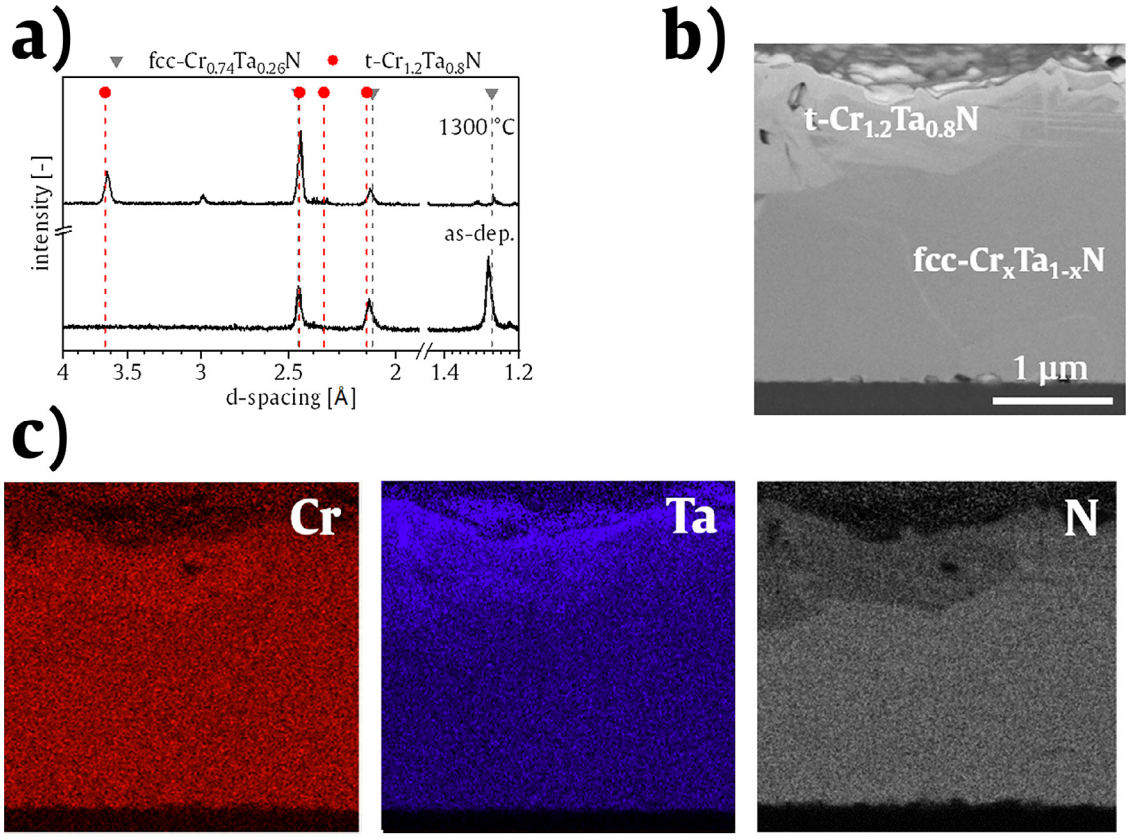

Fig. 7. (a) X-ray diffractogram of CrTaN on sapphire after annealing at 1300°C. The diffractogram of the coating in as-deposited state is shown again to facilitate the comparison. (b) Cross-sectional scanning electron micrograph of the coating after annealing at 1300°C. c) EDX elemental maps of Cr (red), Ta (blue) and N (grey). (For interpretation of the references to color in this figure legend, the reader is referred to the web version of this article.).

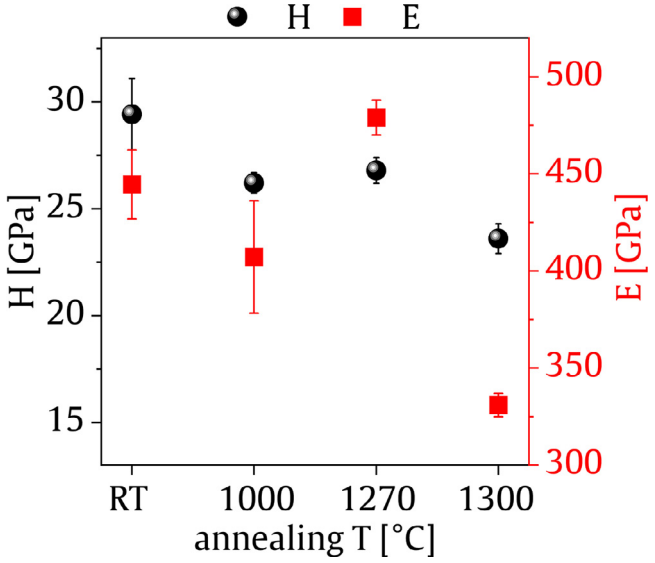

Fig. 8. Hardness and Young's modulus of CrTaN coatings on sapphire substrate in as-deposited state (RT) and after annealing at 1000, 1270 and 1300°C.

4. Conclusions

A complementary application of crystallographic, calorimetric and microscopic characterization techniques allowed to study the thermal stability of a $Cr_{0.74}Ta_{0.26}N$ coating deposited by cathodic arc evaporation. The coating crystallizes in an fcc-$Cr_xTa_{1-x}N$ solid solution with a preferred <311> orientation. Compositional heterogeneous nano-layers in the cross-section of the coating can be attributed to the three-fold rotation applied during deposition. High-energy X-ray diffraction at a synchrotron radiation facility showed that annealing in vacuum to ~1250°C does not alter the phase composition of the powdered coating. Upon further increasing the temperature, the fcc-$Cr_xTa_{1-x}N$ solid solution transforms into t-$Cr_{1.2}Ta_{0.8}N$, followed by the emergence of h-Cr_2N and h-Ta_5N_4. Annealing CrTaN on sapphire in vacuum at 1000°C results in minor grain coarsening and loss of the nano-layers. An annealing temperature of 1270°C provokes major grain coarsening and a texture change from <311> in the as-deposited to <100> in the heat-treated state. Annealing CrTaN on sapphire at 1300°C induces the formation of t-$Cr_{1.2}Ta_{0.8}N$, which is accompanied by a reduction of the hardness. The results gathered within this study confirm the exceptional thermal stability of CrTaN coatings and thus substantiate the high potential of this material for demanding applications.

Declaration of Competing Interest

The authors declare that they have no known competing financial interests or personal relationships that could have appeared to influence the work reported in this paper.

Acknowledgements

The financial support by the Austrian Federal Ministry for Digital and Economic Affairs and the National Foundation for Research, Technology and Development is gratefully acknowledged. The authors thank Dr. Jarosław Wosik, Dr. Julian Wagner (both Materials Center Leoben) and Ing. Gerhard Hawranek (Montanuniversität Leoben) for SEM/FIB/EDX work. Furthermore, we want to express our gratitude to DI Helene Waldl

for assistance in the APT measurements. We acknowledge DESY (Hamburg, Germany), a member of the Helmholtz Association HGF, for the provision of experimental facilities.

References

[1] H. Willmann, P.H. Mayrhofer, P.O.Å. Persson, A.E. Reiter, L. Hultman, C. Mitterer, Thermal stability of Al–Cr–N hard coatings, Scr. Mater. 54 (2006) 1847–1851.

[2] H. Willmann, P.H. Mayrhofer, L. Hultman, C. Mitterer, Thermal stability and age hardening of supersaturated AlCrN hard coatings, Int. Heat Treat. Surf. Eng. 1 (2007) 75–79.

[3] P.H. Mayrhofer, H. Willmann, A.E. Reiter, Structure and phase evolution of Cr–Al–N coatings during annealing, Surf. Coat. Technol. 202 (2008) 4935–4938.

[4] N. Koutná, D. Holec, O. Svoboda, F.F. Klimashin, P.H. Mayrhofer, Point defects stabilise cubic Mo-N and Ta-N, J. Phys. D 49 (2016) 375303.

[5] Y.-I. Chen, Y.-T. Lin, L.-C. Chang, J.-W. Lee, Preparation and annealing study of CrTaN coatings on WC-Co, Surf. Coat. Technol. 206 (2011) 1640–1647.

[6] Y.-I. Chen, K.-Y. Lin, H.-H. Wang, K.-C. Lin, Thermal stability of TaN, CrTaN, TaSiN, and CrTaSiN hard coatings in oxygen-containing atmospheres, Surf. Coat. Technol. 259 (2014) 159–166.

[7] M. Cekada, P. Panjan, B. Navinsek, F. Cvelbar, Characterization of (Cr,Ta)N hard coatings reactively sputtered at low temperature, Vacuum 52 (1999) 461–467.

[8] N. Schalk, M. Pohler, S. Hirn, V.T. Terziyska, P. Polcik, S. Kolozsvári, C. Mitterer, C. Czettl, Microstructure, mechanical properties and cutting performance of $Cr_{1-y}Ta_yN$ single layer and $Ti_{1-x}Al_xN/Cr_{1-y}Ta_yN$ multilayer coatings, Int. J. Refract. Met. Hard Mater. 71 (2018) 211–216.

[9] C. Kainz, C. Saringer, M. Burtscher, M. Tkadletz, A. Stark, N. Schell, M. Pohler, C. Czettl, D. Kiener, N. Schalk, Oxidation resistance of cathodic arc evaporated $Cr_{0.74}Ta_{0.26}N$ coatings, Scr. Mater. 211 (2022) 114492.

[10] C. Kainz, M. Pohler, G.C. Gruber, M. Tkadletz, A.S. Ebner, C. Czettl, N. Schalk, Influence of bias voltage on microstructure, mechanical properties and thermal stability of arc evaporated $C_{r0.74}Ta_{0.26}N$ coatings, Surf. Coat. Technol. 417 (2021) 127212.

[11] W. Ernst, J. Neidhardt, H. Willmann, B. Sartory, P.H. Mayrhofer, C. Mitterer, Thermal decomposition routes of CrN hard coatings synthesized by reactive arc evaporation and magnetron sputtering, Thin Solid Films 517 (2008) 568–574.

[12] F.D. Lai, J.K. Wu, High temperature and corrosion properties of cathodic-arc-plasma-deposited CrN coatings, Surf. Coat. Technol. 64 (1994) 53–57.

[13] C. Héau, R.Y. Fillit, F. Vaux, F. Pascaretti, Study of thermal stability of some hard nitride coatings deposited by reactive magnetron sputtering, Surf. Coat. Technol. 120-121 (1999) 200–205.

[14] A. Thobor-Keck, F. Lapostolle, A.S. Dehlinger, D. Pilloud, J.F. Pierson, C. Coddet, Influence of silicon addition on the oxidation resistance of CrN coatings, Surf. Coat. Technol. 200 (2005) 264–268.

[15] M. Kawate, A. Kimura, T. Suzuki, Microhardness and lattice parameter of $Cr_{1-x}Al_xN$ films, J. Vac. Sci. Technol. A 20 (2002) 569–571.

[16] L. Zhou, D. Holec, P.H. Mayrhofer, Ab initio study of the alloying effect of transition metals on structure, stability and ductility of CrN, J. Phys. D: Appl. Phys. 46 (2013) 365301.

[17] J. Almer, U. Lienert, R.L. Peng, C. Schlauer, M. Odén, Strain and texture analysis of coatings using high-energy X-rays, J. Appl. Phys. 94 (2003) 697–702.

[18] J. Chang, G.-P. Zhao, X.-L. Zhou, K. Liu, L.-Y. Lu, Structure and mechanical properties of tantalum mononitride under highpressure: a first-principles study, J. Appl. Phys. 112 (2012) 083519.

[19] F. Bachmann, R. Hielscher, H. Schaeben, Texture analysis with MTEX – free and open source software toolbox, Solid State Phenom. 160 (2010) 63–68.

[20] N. Schell, A. King, F. Beckmann, T. Fischer, M. Müller, A. Schreyer, The high energy materials science beamline (HEMS) at PETRA III, MSF 772 (2013) 57–61.

[21] M. Basham, J. Filik, M.T. Wharmby, P.C.Y. Chang, B. El Kassaby, M. Gerring, J. Aishima, K. Levik, B.C.A. Pulford, I. Sikharulidze, D. Sneddon, M. Webber, S.S. Dhesi, F. Maccherozzi, O. Svensson, S. Brockhauser, G. Náray, A.W. Ashton, Data Analysis WorkbeNch (DAWN), J. Synchrotron Radiat. 22 (2015) 853–858.

[22] R.A. Young, The Rietveld Method, Oxford University Press, Oxford, New York, 1993.

[23] C. Saringer, M. Tkadletz, A. Stark, N. Schell, C. Czettl, N. Schalk, In-situ investigation of the oxidation behavior of metastable CVD-$Ti_{1-x}Al_xN$ using a novel combination of synchrotron radiation XRD and DSC, Surf. Coat. Technol. 374 (2019) 617–624.

[24] K. Thompson, D. Lawrence, D.J. Larson, J.D. Olson, T.F. Kelly, B. Gorman, In situ site-specific specimen preparation for atom probe tomography, Ultramicroscopy 107 (2007) 131–139.

[25] W.C. Oliver, G.M. Pharr, An improved technique for determining hardness and elastic modulus using load and displacement sensing indentation experiments, J. Mater. Res. 7 (1992) 1564–1583.

[26] M. Widenmeyer, E. Meissner, A. Senyshyn, R. Niewa, On the formation mechanism of chromium nitrides an in situ study, Z. Anorg. Allg. Chem. 640 (2014) 2801.

[27] T. Mashimo, S. Tashiro, T. Toya, M. Nishida, H. Yamazaki, S. Yamaya, K. Oh-ishi, Y. Syono, Synthesis of the B1-type tantalum nitride by shock compression, J. Mater. Sci. 28 (1993) 3439–3443.

[28] P.B. Barna, M. Adamik, J. Lábár, L. Kövér, J. Tóth, A. Dévényi, R. Manaila, Formation of polycrystalline and microcrystalline composite thin films by codeposition and surface chemical reaction, Surf. Coat. Technol. 125 (2000) 147–150.

[29] M. Hans, M. to Baben, Y.-T. Chen, K.G. Pradeep, D.M. Holzapfel, D. Primetzhofer, D. Kurapov, J. Ramm, M. Arndt, H. Rudigier, J.M. Schneider, Substrate rotation-induced chemical modulation in Ti-Al-O-N coatings synthesized by cathodic arc in an industrial deposition plant, Surf. Coat. Technol. 305 (2016) 249–253.

[30] M. Panjan, Influence of substrate rotation and target arrangement on the periodicity and uniformity of layered coatings, Surf. Coat. Technol. 235 (2013) 32–44.

[31] P. Ettmayer, Die Struktur der Komplexnitride NbCrN und $Ta_{1-x}Cr_{1+x}N$, Monatsh. Chem. 102 (1971).

[32] N. Jäger, M. Meindlhumer, S. Spor, H. Hruby, J. Julin, A. Stark, F. Nahif, J. Keckes, C. Mitterer, R. Daniel, Microstructural evolution and thermal stability of AlCr(Si)N hard coatings revealed by in-situ high-temperature high-energy grazing incidence transmission X-ray diffraction, Acta Mater. 186 (2020) 545–554.

[33] C. Hu, Y.X. Xu, L. Chen, F. Pei, Y. Du, Mechanical properties, thermal stability and oxidation resistance of Ta-doped CrAlN coatings, Surf. Coat. Technol. 368 (2019) 25–32.

[34] M.C. Morris, H.F. McMurdie, E.H. Evans, B. Paretzkin, H.S. Parker, W. Wong-Ng, D.M. Gladhill, C.R. Hubbard, Standard X-ray Diffraction Powder Patterns, 25th ed., 1985.

[35] Fiala, Central Research Institute, SKODA, Czechoslovakia, 1973.

[36] C. Kainz, M. Pohler, M. Tkadletz, C. Czettl, N. Schalk, The influence of bias voltage on structure, thermal stability and mechanical properties of arc evaporated $Cr_{0.69}Ta_{0.20}B_{0.11}N$ coatings, Surf. Coat. Technol. 428 (2021) 127867.

[37] B.D. Cullity, Elements of X-ray Diffraction, Addison-Wesley, Reading Massachusetts, 1978.

[38] C.M. Koller, A. Kirnbauer, R. Rachbauer, S. Kolozsvári, P.H. Mayrhofer, Thermally-induced phase transformation sequence of arc evaporated Ta–Al–N coatings, Scr. Mater. 113 (2016) 75–78.

[39] Q.M. Wang, K.H. Kim, Effect of negative bias voltage on CrN films deposited by arc ion plating. II. Film composition, structure, and properties, J. Vac. Sci. Technol. A 26 (2008) 1267–1276.

[40] J. Pelleg, L.Z. Zevin, S. Lungo, N. Croitoru, Reactive-sputter-deposited TiN films on glass substrates, Thin Solid Films 197 (1991) 117–128.